Rock mechanics of the Davis Detector Cavern

W.G. Pariseau
Professor emeritus, University of Utah, Salt Lake City, UT

D.R. Tesarik
Mechanical engineer, Office of Mine Safety and Health Research, Spokane Research Laboratory, National Institute for Occupational Safety and Health, Spokane, WA

T.C. Trancynger
Geologist, Sanford Underground Science and Engineering Laboratory at Homestake, Lead, SD

Abstract

The Davis detector cavern was excavated on the 4850 Level of the former Homestake Mine in the mid-1960s to house a novel neutrino detector developed by Nobel Prize winner Dr. R. Davis. The original cavern was about 9.1 x 16.8 x 9.7 m high, excavated in a Precambrian amphibolite known as the Yates unit and enlarged in 2010. In 2009, the National Science Foundation selected the site for development as a national Deep Underground Science and Engineering Laboratory (DUSEL). This retrospective rock mechanics study of the Davis cavern is intended to inform design of the much larger caverns and laboratory rooms being considered for the same 4850 Level. Provision for rock mass variability, sequential excavation, jointing and wall damage from blasting are included in analyses that were done using two different computer codes and methods (FLAC3D and UTAH3). The results are in agreement with observations and show that cavern stability is indeed the case. The main conclusions are: (1) if conventional scaling of laboratory rock elastic moduli and strengths is done, then 0.25 and 0.50 scale factors are reasonable, (2) measured statistical and spatial variability in rock properties should be incorporated into geomechanical analyses to better reflect reality, (3) discontinuities ("joints") are essential to reliable analysis of excavation safety and when properly taken into account eliminate the need for empirical "scaling" of laboratory rock properties, (4) major geologic features such as rhyolite dikes and breccia zones may be important to excavation safety at Homestake and should be explicitly represented in analyses and (5) quantifying wall blast damage is important to engineering design of underground excavations.

Key words: Homestake Mine, DUSEL, Deep Underground Science and Engineering Laboratory, Rock mechanics, Modeling and simulation

2012 *Transactions of the Society for Mining, Metallurgy, and Exploration*, Vol. 332, pp. 370-388.

Introduction

This contribution describes rock mechanics features of the Davis Cavern at the former Homestake Mine in Lead, SD. The mine is located in the northern Black Hills of South Dakota. In 2003 and again in 2008, the mine site was recommended for development as a national Deep Underground Science and Engineering Laboratory (DUSEL) in cooperation with the Sanford Underground Science and Engineering Laboratory under the South Dakota Science and Technology Authority (SDSTA). The original Davis Cavern was excavated about 9.1 x 16.8 x 9.7 m high (30 x 55 x 32 ft high) in 1965 (Mitchell, 2009) at a depth of 1,478 m (4,850 ft). The purpose of the cavern was to house apparatus for detecting solar neutrinos. The experiment ultimately proved successful and earned R. Davis a share of the 2002 Nobel Prize in physics. Recently, a new experiment (involving the large underground xenon detector, or LUX, for dark matter particles and weakly interacting massive particles, or WIMPs) was proposed for the Davis Cavern that required an increase in height of 2.4 m (8 ft).

For many years, the Homestake Gold Mine was the deepest operating mine in North America. Development extended to the 8000 Level (2,438 m). The mine closed in 2003. Pumps were shut off and the water level rose to the 4350 Level, about 150 m (500 ft) above the Davis Cavern. About six years later, after selection for DUSEL proposal development by the National Science Foundation (NSF), access to the 4850 Level and the Davis Cavern was regained. Pumping has lowered the water level to well below the cavern floor. Figure 1 shows the layout and location of the Davis Cavern. The detector tank, supporting steel and so forth were subsequently removed. Next, the cavern was resupported and new access was developed. By August, 2010, 368 m^3 (13,000 ft^3) had been removed during

Paper number TP-12-010. Original manuscript submitted February 2012. Revised manuscript accepted for publication September 2012. Discussion of this peer-reviewed and approved paper is invited and must be submitted to SME Publications Dept. prior to Sept. 30, 2013.

enlargement and renovation of the Davis Cavern. Figure 2 shows the detector tank under construction in 1965.

A number of rock mechanics studies were done at the Homestake Mine beginning in the 1980s (Pariseau, 1985; Pariseau et al., 1995, 1996). A large accumulation of rock properties and stress measurement data was developed in the course of these studies, which focused on rock formations important to gold mining in the Poorman, Homestake and Ellison formations. All are Precambrian metasediments. The Davis Cavern is located in the Yates member of the Poorman formation away from any active mining region. Although the Yates member is considered strong and massive, little quantitative data were available for design analysis. The presence of Tertiary rhyolite intrusives complicates the geologic setting. However, the fact that the cavern has been stable for more than 40 years suggested that increasing cavern height by 2.4 m (8 ft) to 12.1 m from 9.7 m (to 40 ft from 32 ft) could be safely done.

Rock mechanic investigations for DUSEL, with focus on very large water-Cherenkov and other neutrino detector caverns and large laboratory rooms, provided new data about the Yates formation. These investigations include study of geology, hydrogeology, structure, access drift and cavern mapping, borehole televiewing and core logging, laser scanning of the new cavern, point load testing, laboratory testing for rock and discontinuity properties (mechanical), and in situ stress measurement (Hladysz et al., 2011). Data from these investigations provided a portion of the input data needed for retrospective design analysis of the old and new Davis Caverns. Although a small but persistent seep is present in the west wall of the cavern, the effect is insignificant and the rock mass was considered dry. Both rock types (Yates amphibolite, Tertiary rhyolite) were considered isotropic. A photograph of the new, enlarged Davis Cavern is shown in Fig. 3.

The objectives of the analyses were: (1) to estimate calibration or scale factors for elastic moduli and strengths, (2) to develop a quantitative understanding of the effect of randomness or variability in rock properties, (3) to assess the role of joints and (4) to assess the influence of blasting on cavern walls. Two numerical methods and computer programs were used

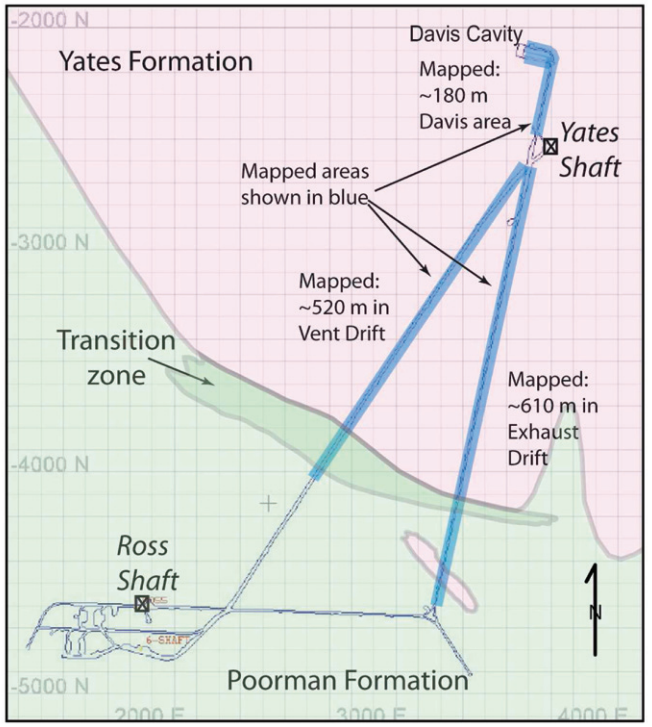

Figure 1 — Location of the Davis Cavern (Davis Cavity) on the 4850 Level of the Sanford Laboratory at Homestake (Hladysz et al., 2011).

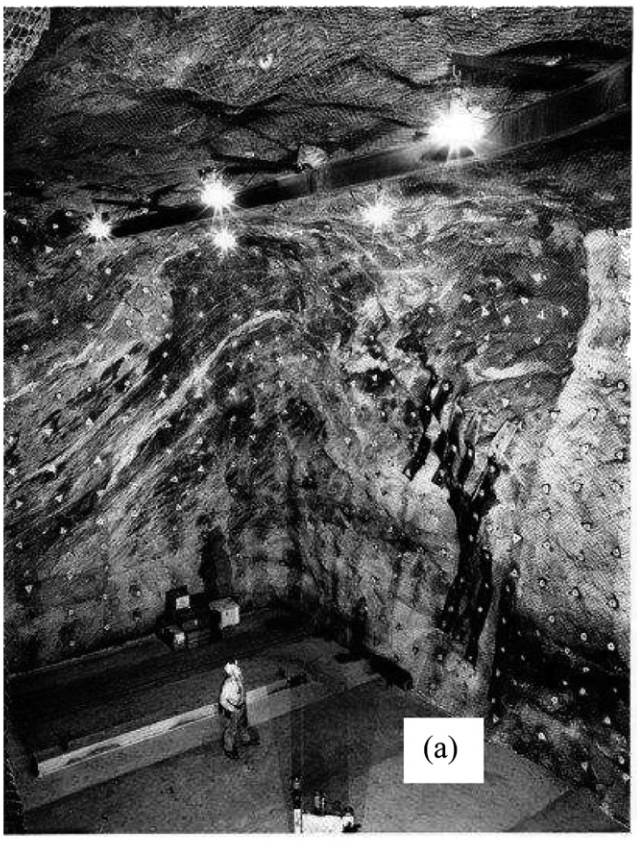

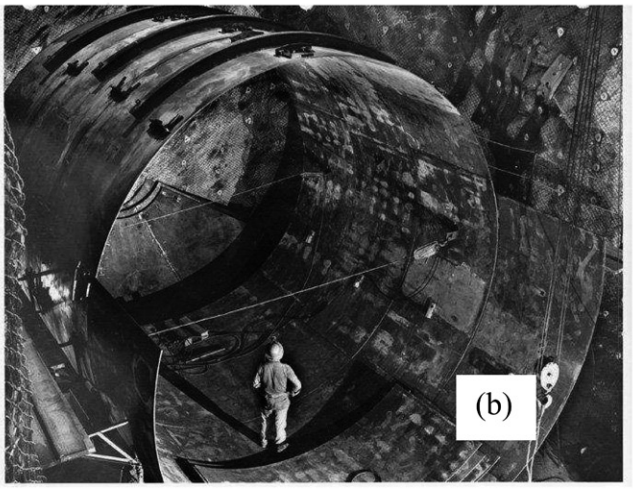

Figure 2 — Photographs of the original Davis Cavern and construction of the detector tank in 1965. Mechanical bolts and some straps were used for surface support; (a) cavern corner and (b) detector tank.

Figure 3 — The enlarged, new Davis Cavern looking south with a new access drift clearly visible.

for the analyses: the popular finite difference FLAC3D Itasca code (Itasca, 2006) and the finite element (FE) code UTAH3, which has been in use for many years. FLAC3D was used to examine the effects of blasting on cavern walls, while UTAH3 was used to estimate scale factors and to examine the effects of randomness on cavern safety. In this regard, laboratory test cores were obtained from drill holes collared in the Vent Drift (Fig. 1) that are not in the immediate vicinity of the cavern, as would be desirable. Additionally, an extensometer plan to monitor displacements induced by cavern enlargement was not successful; therefore, this retrospective analysis of Davis Cavern stability is only semiquantitative. However, establishing lower bounds to rock mass properties should be useful for constraining analyses of future excavations in the Yates formation in the region of the 4850 Level.

Input data

The main input data sets for each analysis are similar, although not identical, and consist of geology and structure, rock properties, preexcavation stress state and excavation sequence. These data are represented in finite element (FE) and finite difference models where element and cell size are a compromise between the desire for accurate detection of stress concentration near excavation walls and the practical advantage of short run times. The differences in analyses input data details are described as they are encountered.

Geology and structure. The main rock types present at the Homestake site are Precambrian metasediments in the Poorman, Homestake and Ellison formations. These formations exist in a series of northwesterly isoclinal folds that plunge to the southeast (Slaughter, 1968). A second stage of cross folding may be associated with Tertiary intrusives. The Poorman and Ellison formations are highly foliated phyllites and schists, while the Homestake formation hosts gold mineralization, quartz lenses and is not nearly so foliated as the older Poorman and younger Ellison formations.

An important unit is the Yates member of the Poorman formation, an amphibolite, which is the oldest unit present. The Yates unit is considered massive and strong and is thus a promising host rock for the large and deep caverns and rooms proposed for the laboratory. There are variations within formations and within the Yates member, especially near contacts between rock types. Moreover, folding occurs at a multiplicity of scales, ranging from centimeters to meters to kilometers, and is most evident in the foliated Poorman formation, although less so in the Yates member. Faults are present to some degree, show relatively small offsets and are generally annealed, and thus do not pose any particular hazard to ground control or safety.

Tertiary rhyolites have intruded all formations and are present from the surface to the 7400 Level and at greater depths. These intrusions occur in dike swarms and vary greatly in thickness and continuity. Several types of rhyolites are recognized and occur in discontinuous dikes that may be concordant with structure, but not always. Test cylinders of amphibolite and rhyolite failed violently, with little indication of approach to failure during a laboratory compressive strength study.

Rock and joint properties. Material behavior was considered linearly elastic with the limit to elasticity defined by an N-type failure criterion (Pariseau, 1967) in FE analysis and the linear Drucker-Prager criterion in FLAC analyses. Both

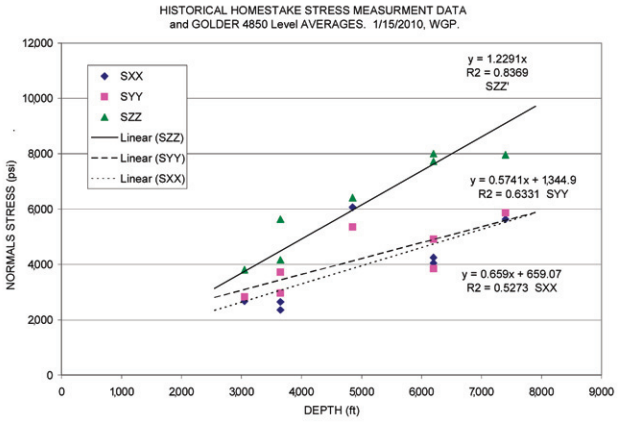

Figure 4 — Normal stress-depth measurements and trend lines at the Homestake laboratory.

Table 1 — Combined rhyolite laboratory test results.

Property statistic	E (GPa)	ν	γ (kN/m^3)	T_o (MPa)	C_o (MPa)
Number	32	18	39	48	32
Mean	54	0.20	28	12	156
Stdev	11	0.03	2	3	88
Cv%	20%	15%	7%	28%	57%
Stdm	3	0.01	0	1	24
High	76	0.25	-	21	369
Low	26	0.15	-	5	28

Number = number of tests, mean = arithmetic mean of the samples, stdev = standard deviation, cv% = coefficient of variation (%), stdm = standard deviation of the mean, high = maximum value, low = minimum value, E = Young's modulus, ν = Poisson's ratio, γ = specific weight, T_o = tensile strength, C_o = unconfined compressive strength.

have a simple form: $J_2^{N/2} + I_1 = 1$, where the first term is an anisotropic form of the second invariant of stress; the second term is an anisotropic form of the first invariant of stress, the exponent $N = 2$ in the finite element analyses; while $N = 1$ when the isotropic Drucker-Prager criterion ($J_2^{1/2} = AI_1 + B$) is used (compression positive here). The strength constants A and B may be obtained from unconfined compressive and tensile strength. Normal stresses are total stresses and, in view of the "dry" condition, are also effective stresses. A discussion of anisotropy (orthotropy) and the N-type criterion is given by Pariseau (1972). In this regard, although isotropy is assumed for intact rock and discontinuities ("joints"), fully anisotropic properties develop when joints are embedded in the FE mesh. Generally, jointed rock masses require fully anisotropic material model capability.

Tables 1 and 2 contain rock properties used in finite element analyses with values rounded off. Properties of rhyolite and amphibolite are a combined data set obtained from a merger of laboratory test data generated by RESPEC, Inc., and the University of Utah (Hladysz et al., 2011; Pariseau et al., 2010). Test cores were obtained at some distance from the Davis Cavern. University of Utah cores were obtained from drill hole N, while RESPEC data were obtained from drift walls on the 4850 Level.

In the jointed rock mass FE analyses, joint properties were

Table 2 — Combined amphibolite laboratory test results.

Property statistic	E (GPa)	ν	γ (kN/m^3)	T_o (MPa)	C_o (MPa)
Number	30	18	48	77	48
Mean	84	0.25	29	11	124
Stdev	20	0.04	1	5	55
Cv%	23%	16%	3%	47%	45%
Stdm	4	0.01	0	0	14
High	153	0.36	-	35	235
Low	54	0.19	-	0	33

Table 3 — Joint set orientation and spacing.

Feature joint set	Dip direction (azimuth-deg)	Dip (deg)	Spacing (m)
1	120	36	1.0
2	216	52	0.5
3	261	74	0.8
4	358	58	1.7

estimated as 1/100th of intact rock properties for lack of actual measurements of joint stiffnesses and strengths. A ratio of 1/1,000 would be equally valid under the circumstances. For example, E (joint) = E (rock)/100 and T_o (joint) = T_o (rock)/100, but ν (joint) = ν (rock) and ϕ (joint) = ϕ (rock), where ϕ = angle of internal friction. The last follows from the fact that the ratio $r = C_o / T_o$ for rock and joint is the same dimensionless quantity. In case of a Mohr-Coulomb failure criterion, one has $\sin(\varphi) = (C_o - T_o)/(C_o + T_o)$ and for cohesion, $c = \sqrt{C_o T_o / 4}$. Joints have not been sampled, nor have joint strengths and stiffnesses been measured, so assumptions were necessary to proceed.

Four discontinuities or "joint" sets were recognized (Golder Associates, 2010a). Table 3 shows joint set orientation and spacing averages. Variability is present in the data, and ranges of dip, dip direction and spacing are considerable. Joint persistence useful for estimating joint rock strength is the ratio of bridge area to total area ($p = A_j / (A_j + A_r)$, where j = joint and r = rock), is unknown. An indicator of this persistence is the ratio of bridge length to total length, but this is also unknown. Both are likely to be variable in any case.

Preexcavation stress. A variety of methods were used by different investigators to measure the in situ state of stress at the Homestake Mine (Pariseau, 1985). These measurements ranged from the 3050 Level to the 7400 Level. Generally, the major principal stress is near vertical, while the intermediate and minor principal stresses aligned across and parallel with major structural trends. Compass coordinates for analysis are nearly aligned with structural trends. Simple formulas consistent with these measurements indicated that with compression positive and stress in psi,

$$S_H = 2078 + 0.53h$$
$$S_h = 121 + 0.55h \qquad (1)$$
$$S_v = 1.25h$$

where h = depth (ft), S_H = normal stress in the dip direction, S_h = normal stress in the strike direction and S_v = vertical stress.

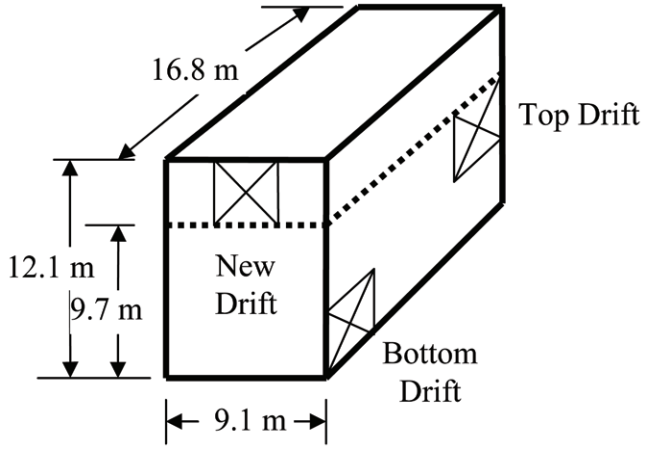

Figure 5 — A schematic of the original and enlarged Davis Cavern.

When the stresses were referred to compass coordinates (x = east, y = north, z = up), the normal stresses were an order of magnitude greater than the shear stresses. Figure 4 is a plot of normal stresses in compass coordinates versus depth.

Recently, stress measurements were made by Golder Associates on the 4850 Level in connection with the DUSEL effort (Golder Associates, 2010b). The averaged normal stress data from these measurements are also in the plot. All measurements indicate small shear stresses relative to normal stresses referred to compass coordinates. The trend lines in the plot give about the same S_v and S_H values, while the trend line value of S_h is noticeably greater than the value from the formulas based on historic data. Because greater differences among principal stresses lead to greater stress concentrations, a conservative approach is to use the historical formulas to estimate the preexcavation stress field. Thus, on the 4850 Level, the preexcavation normal stresses in MPa were S_H = 32.1, S_h = 19.2, and S_v = 41.8; preexcavation shear stresses were neglected. Here $H = x$ = east, $h = y$ = north, and v = up = vertical, and compression is positive.

Excavation sequence. The actual excavation sequence of the original Davis Cavern in 1965 is not known, but a reasonable breakdown of major stages is: (1) excavation of a top drift from the 4850 Level, (2) excavation of the decline or bottom drift, (3) excavation of the original Davis Cavern, (4) excavation of the new Davis Cavern and (5) excavation of a new drift from the 4850 Level. The original top drift penetrates the original Davis Cavern at the cavern top, near the northeast corner of the east wall. The decline penetrates the original cavern at the bottom of the cavern, near the southeast corner of the east wall. The new Davis Cavern is about 2.4 m (8 ft) higher than the original cavern, and the new drift penetrates the new Davis Cavern near the top of the center of the south wall. Figure 5 is a schematic that shows the approximate dimensions of the access drifts to the original Davis Cavern and the new, enlarged cavern. Because the cavern was stable during the original excavation sequence and is stable today, one infers that deformations associated with past and recent excavations are in the elastic range. Consequently, the excavation sequence was expected to be of little consequence.

Scale factors

Scale factors here refer to numbers on the interval [0,1] that are used to multiply centimeter-scale laboratory values of elastic moduli and strengths to estimate corresponding values at the engineering or field scale of meters. Differences in properties associated with "scale" are attributed to discontinuities or defects that are present in the field-scale rock mass, but absent in laboratory-scale test specimens. To be sure, conventional wisdom states that discontinuities such as faults, fractures, bedding planes and joints make the rock mass more compliant and weaker.

A common procedure for estimating scale factors is back analysis, which involves comparisons between measured and calculated displacements. The measured displacements are often obtained from multiple position borehole extensometers (MPBXs). Input rock properties are then scaled for analysis. A comparison between calculated MPBX readings and actual readings associated with excavation is then done. Scale factors are adjusted and another analysis is performed. The process continues until satisfactory agreement between measured and calculated readings is obtained or until no further improvement is made. A simple and direct comparison using back analysis data is a plot of calculated versus measured MPBX readings. The slope of a trend line passing through the origin is a scale factor for elastic moduli. If anchor loss occurs, then certainly any zone of inelasticity in the model is constrained by anchor loss position. Any strength scale factor is also constrained by anchor loss. Regression analysis of elastic displacement (linear) indicates a goodness of fit through the correlation coefficient, while the slope of the regression line is a scale factor for elastic moduli. Some discipline can be brought to the process by invoking simple nondimensional scaling rules. For example, under uniaxial loading, strain energy to failure indicates that a strength scale factor (cfac) is just the square root of the elastic modulus scale factor (efac). Thus, if efac = 0.25, then cfac = 0.50. If a simple strain to failure is used as a guide, then the two scale factors are equal. In fact, these values were determined in rock mechanics studies at the Homestake Mine in the course of a shaft pillar study (Pariseau et al., 1995, 1996).

No extensometer data are available for direct estimation of scale factors for the Davis Cavern. However, the cavern has remained stable since excavation in 1965 and, thus, must surely be considered stable. Displacements, strains and stresses associated with excavation are therefore within the elastic domain of response. Long-term displacements associated with creep must also be negligibly small relative to the elastic limit or rupture point. Results from FE and FLAC3D analyses must be consistent with these observations.

Mesh geometry. A three-dimensional, 140,800-element mesh of the Davis Cavern was constructed with 145,737 nodes. Elements are eight-node, constant-strain "bricks." The mesh contains the cavern shown in Fig. 5 and three access drifts that penetrate the cavern. Overall dimensions of the mesh are 33.5 x 61.6 x 44.8 m (110 x 202 x 147 ft) in the x, y and z directions, respectively. The maximum cavern dimension is 16.8 m (55 ft), so the overall mesh dimensions are no less than two times the maximum excavation dimension. If the intermediate excavation dimension of 12.1 m (40 ft) is D, then the least mesh dimension is about 2.75D. Element dimensions are in proportion to the cavern dimensions, except for elements in eight outer shells; each cavern face is represented by 400 (20 x 20) elements. The long cavern dimension (y) is 1.833 times the short dimension (x) and 1.375 times the intermediate dimension (z). Cavern element aspect ratio is thus 1.833. Elements at the cavern walls are about 0.46 x 0.84 x 0.61 m (x, y, z) or 1.5 x 2.75 x 2.0 ft, and provide adequate numerical quality for assessment of cavern safety and stability. In this regard,

rock bolts of moderate length and spacing, say, 1.5 m (5 ft) with wire mesh, readily contain any loose wall rock that may be present but escaped scaling during construction, as seen in Figs. 2 and 3. FE analyses are more concerned with overall cavern safety and the potential for large wall, back and floor failures and possible collapse of the excavation.

Figure 6 shows a plan view (z = 0 coordinate plane) of the mesh; the origin is at the center of the new Davis Cavern. The other coordinate planes are similar, although of different dimensions. Gray elements in the mesh are "cut" elements; these elements are excavated in the course of analysis. The three access drifts in Fig. 5 do not appear in plan view or in cross-section, although the new drift would appear in a long-section through the origin.

Finite element analyses. Several analyses of the Davis Cavern excavation and enlargement were done using constant (average) laboratory rock properties. The first analysis was a comparison between sequential excavation of access drifts and so on and excavation all at once. In the elastic domain, no significant difference is expected, although some differences are possible theoretically and numerically. The sequential excavation proceeded in five steps: (1) excavation of the top drift, (2) excavation of the bottom drift, (3) excavation of the original cavern, (4) excavation enlargement to the height of the new cavern and (5) excavation of the new drift. Figure 7 compares color contours of element safety factors over coordinate planes where stress concentrations would be greatest in the absence of access drifts.

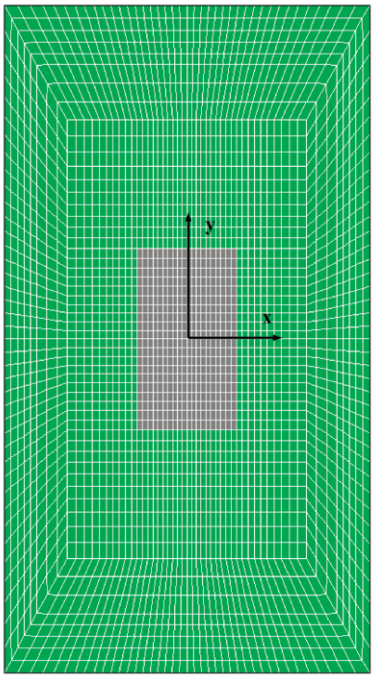

Figure 6 — Mesh elements in the z = 0 coordinate plan view. Gray elements define the Davis Cavern in plan view 9.1 x 16.8 m (30 x 55 ft), or 20 x 20 elements.

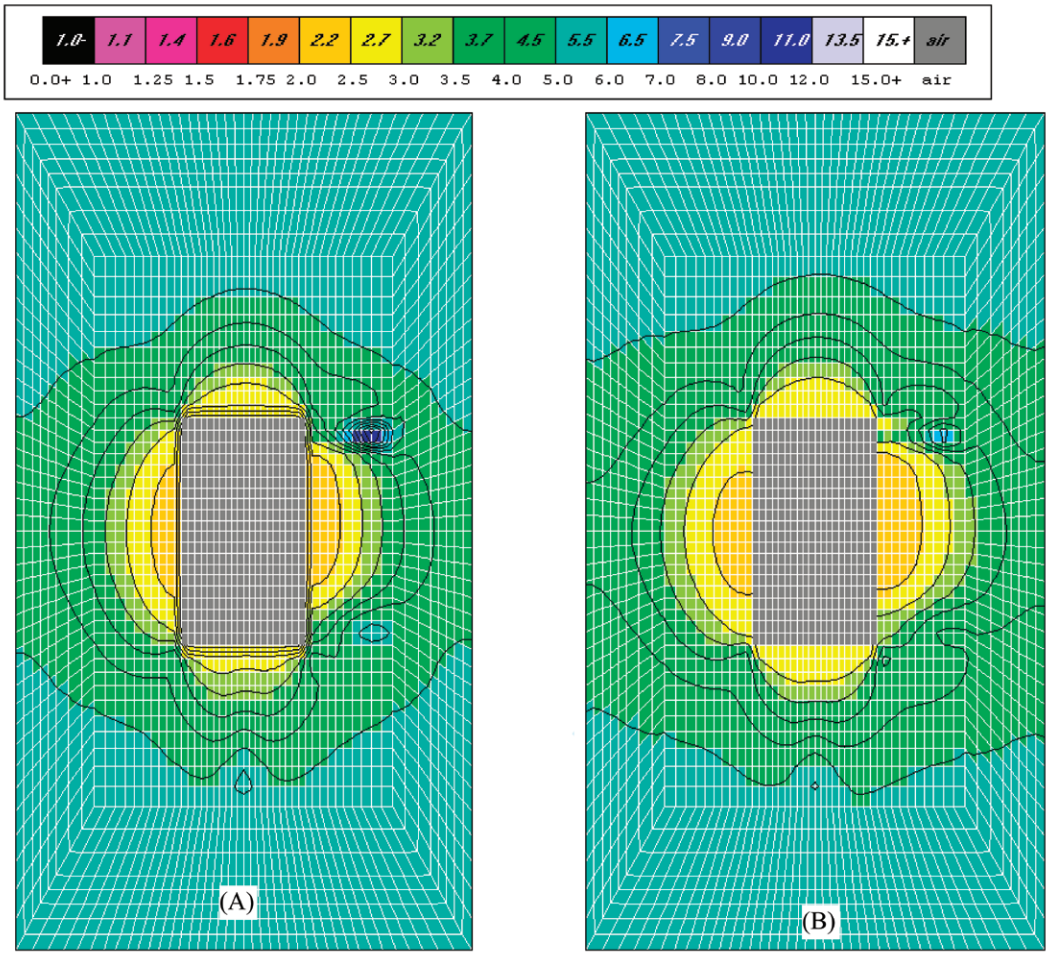

Figure 7 — Plan view (z = 0) of element safety factors: (A) after sequential excavation in five runs and (B) after excavation in a single run.

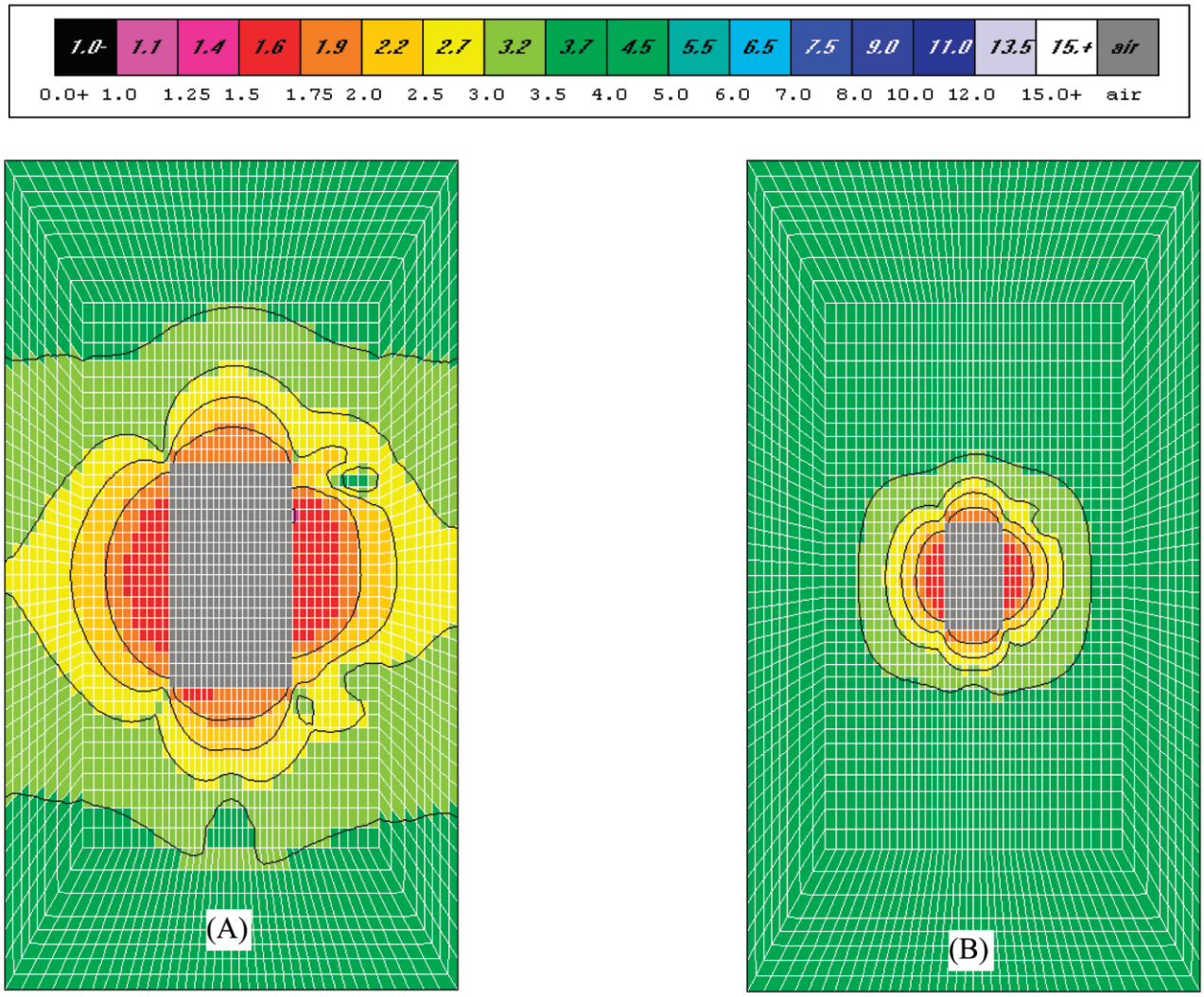

Figure 8 — Outer boundary effect on cavern wall stress concentration: (A) near boundary case and (B) far boundary case. The cavern is the same size in both cases. The $z = 0$ coordinate plane is shown.

The element safety factor *fs* here is defined as a ratio of strength to stress, and is given specifically by the ratio $J_2^{1/2}$ (strength) / $J_2^{1/2}$ (stress), where the numerator is computed from the yield criterion and the denominator is computed from element stresses. Strength is stress-dependent, so the numerator also depends on element stresses. In principal stress space, *fs* is the ratio of the maximum diameter of the circle allowed by the yield condition to the actual diameter of a circle in a plane normal to the hydrostatic axis when the material is isotropic. No element in the data from which Fig. 7 is obtained has a safety factor less than 1.3. A few elements have safety factors greater than 11. These elements are in a shadow zone below the top access drift. *The differences between sequential and single run excavation are slight and, therefore, single-run excavation is sufficient*.

Elements remote from the cavern walls in Fig. 7 have safety factors greater than 4.0, but the distribution of element safety factors near the outer boundary is not uniform. This feature implies an outer boundary effect. The effect is adverse in the sense that the finite distance between cavern walls and the outer boundary tends to increase stress concentration with a broadening of the zone of stress concentration. This effect is seen in Fig. 8. Also seen in Fig. 8 is the result of moduli and strength reduction through scaling of moduli and strengths by factors of 0.25 and 0.5, respectively. A decrease in cavern wall safety factors to near 1.5 from 2.0 occurs as a consequence, although the cavern remains safe. These scale factors are guided by a simple, one-dimensional energy criterion that assumes the energy to failure is independent of scale. As a consequence, $(E_l / E_f) = (C_l / C_f)^2$, where l and f signify laboratory and field scales, E = Young's modulus and C = unconfined compressive strength. No failures are evident in Fig. 8. However, a few elements did fail where the new drift penetrates the new Davis Cavern. In fact, three elements failed on each side of the new drift where it enters the south wall of the cavern. This location of failure is not surprising, because the south wall sees the greatest stress concentration without consideration of access drift penetration. However, the additional concentration of stress occurs about the new access drift. The same phenomenon occurs where the two other access drifts penetrate the cavern east wall, although this wall is less prone to stress concentration than the south wall. Orientation of the cavern axes relative to the preexcavation stress field is the reason.

Figure 9 presents scaled FE results where moduli (Young's modulus, shear modulus) and strength (unconfined compressive and tensile strength) scale factors of 0.25 and 0.5, respectively, are used for comparison with scale factors of 0.16 and 0.4 (moduli, strength, respectively). The unscaled plan view

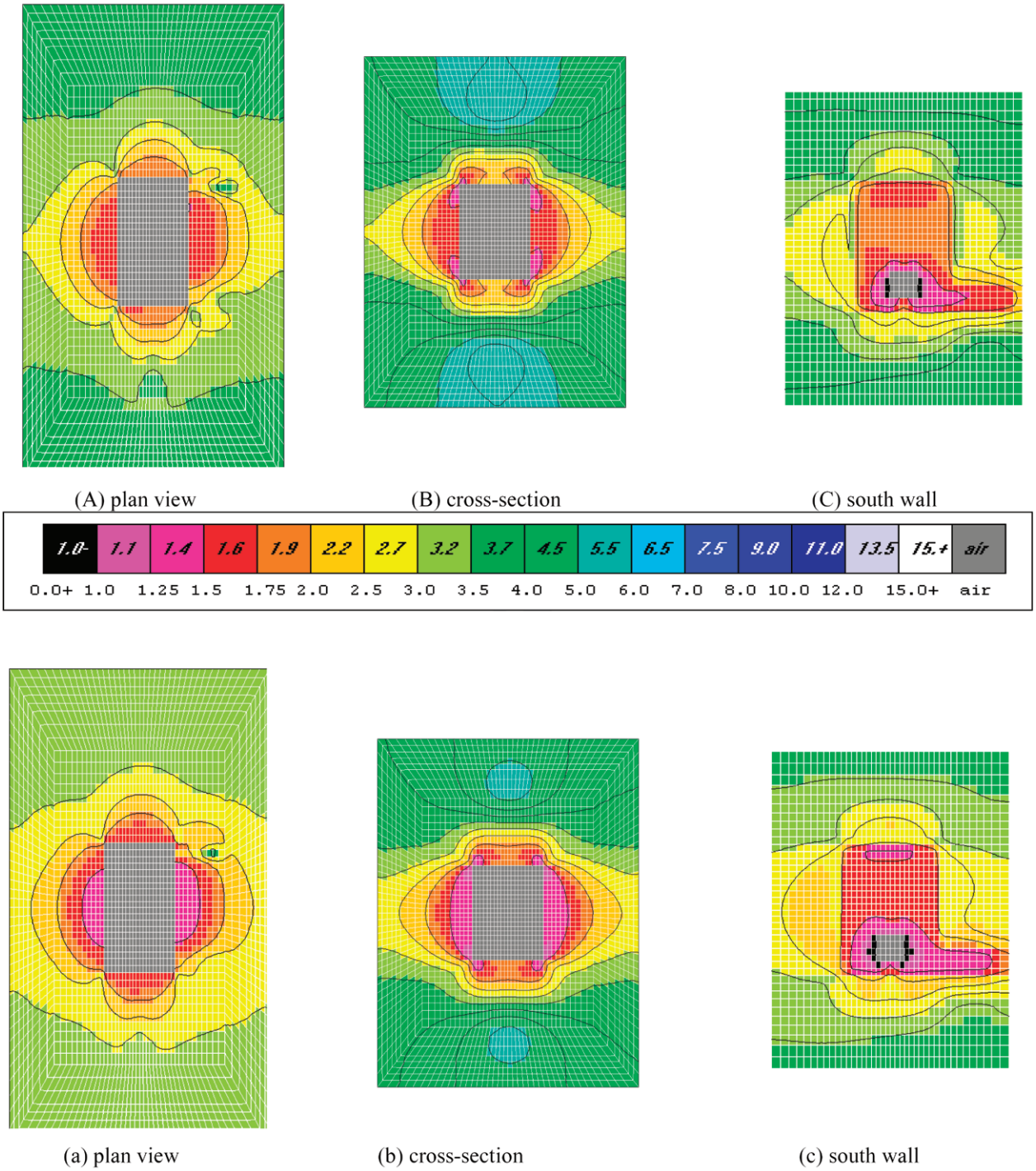

Figure 9 — Element safety factor distributions after excavation using scale factors A, B, C: 0.25 and 0.5 scale factors for elastic moduli and strengths; a,b,c: 0.16 and 0.4 moduli and strength case factors.

distribution of element safety factors is shown in Fig. 7B for comparison.

Consideration of the actual condition of the cavern and the FE results supports a conclusion that scale factors should be no less than 0.25 and 0.5 for moduli and strengths, respectively. These values were just those achieved in previous studies at the Homestake Mine (Pariseau, 1999).

Randomness effects

Variability in rock properties is the rule rather than exception. Laboratory test data often show coefficients of variation in unconfined compressive strength of 35% and more (e.g., Singh, 1981). Similar variability is observed in tensile strength determined from Brazil test data. Even greater variability would be observed if the damaged core was not avoided in selection of core lengths for testing. Including observed variability in numerical models would be a step toward obtaining more realistic results for design guidance. In this regard, a simple thought experiment illustrates the shortcomings of much current design based on average properties. In the case of more

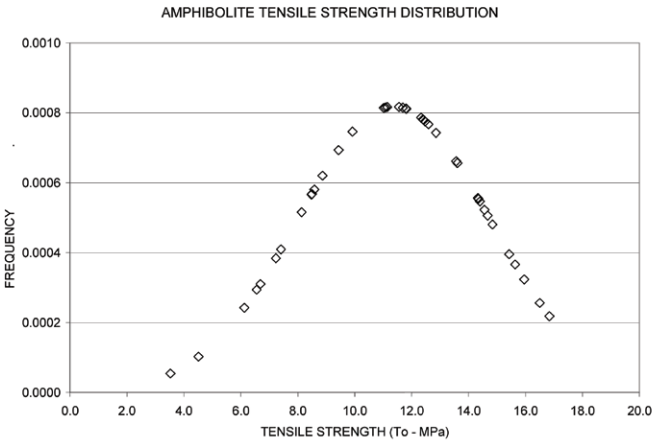

Figure 10 — Frequency distribution of a suite of amphibolite tensile strength data.

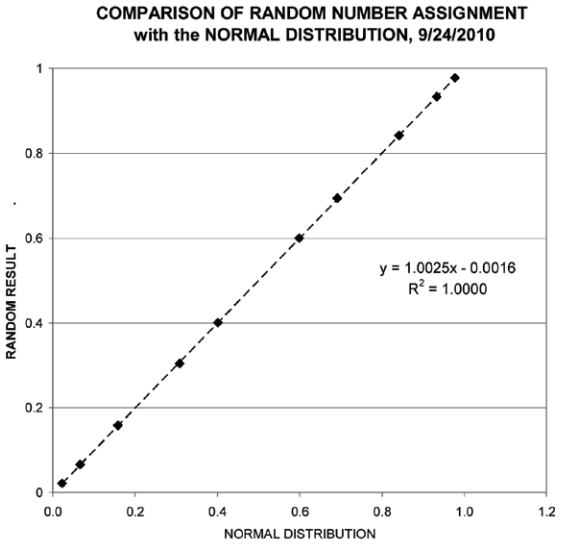

Figure 11 — Comparison of random element properties assignment with a normal distribution in an 80,384-element mesh.

realistic variable properties, some elements in a model would have higher strength, while some would have lower strength. Elements that were "safe" on average would certainly be safe at higher strength, but elements at lower strength may fail. A collapse mechanism could possibly form a path through failing lower strength elements. Thus, randomness may be a major determinant of the need for scale factors in analyses based on average rock properties. Of course, there is also the important role of "joints" to consider. Although probabilistic and statistical characterization of heterogeneous materials has a long history, only in recent years have advances in computational capabilities and reduction in costs allowed for substantial progress in studies of random media in the geotechnical realm (Griffiths and Fenton, 2007). Computational demands are still considerable because of the enormous number of model runs required for definitive results, so some compromise is helpful in illustrating randomness effects.

A conceptual difficulty with the use of scale factors obtained from back analysis is clear in Fig. 9, where all elements in the mesh have reduced moduli and strengths. Random assignment

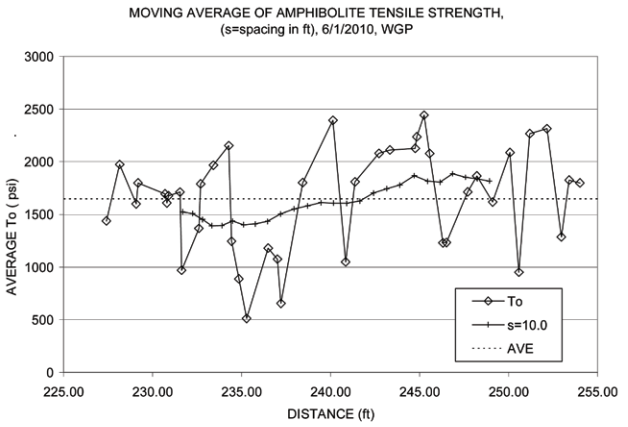

Figure 12 — Tensile strength of amphibolite along a sampling drill hole.

based on observed variability overcomes this drawback.

One approach is to introduce variability observed in laboratory test data into element properties assignment. This seemingly simple task defies rigorous implementation because of numerous statistical relationships that need to be quantified. A practical procedure is to partition data into a number of bins or intervals that mimic the observed distribution of data, perhaps in a histogram. In the present analysis, tensile strength from Brazil test data was partitioned into 11 bins, 5 above and 5 below the mean. This partition was done under the assumption of a normal distribution with clipped tails that avoided infinite and negative tensile strengths. Other distributions were also considered, including the lognormal distribution and three-parameter Weibull distributions. There was little difference in best fits over the range of observed data. Figure 10 shows the frequency distribution of a suite of 41 tensile strength tests. A visual inspection indicates a roughly symmetric distribution about the mean in keeping with a normal distribution. There is suggestion of a small negative skew, but further exploration of the data show a very slight positive skew. If the skew were large, then a non-normal distribution would be needed and would be conditioned by the sign of the skew. Figure 11 shows a comparison of element properties assignment in a mesh of 80,384 elements with a normal distribution. The fit is excellent and indicates proper functioning of the properties assignment procedure.

A random number drawn on the interval (0,1) is used to assign a material type to the element. Each material type corresponds to a material property set defined by a tensile strength (T_o) that is decreased or increased from the mean value according to the input distribution. The ratio of unconfined compressive to tensile strength (C_o/T_o) is kept constant. The ratio of Young's modulus to shear modulus (E/G) and Poisson's ratio (ν) are also kept constant. If an assignment produces $T_o = 0.375T_o$(average), then $E = 0.375E$(average) and $C_o = 0.375C_o$(average), $G = 0.375G$(average) and so on. Perfect correlations are implied in this process.

Evidence of spatial variability of properties becomes quite clear when laboratory sample test data are related back to physical locations at the Homestake site. Figure 12 shows tensile strength along a length of HQ3 diamond drill hole collared on the 4850 Level. Rapid fluctuation about the sample set mean is clearly evident. The diamond symbol indicates laboratory test data, while the small, vertical bar signifies a moving average based on a spacing of 10 ft. A correlation length or distance,

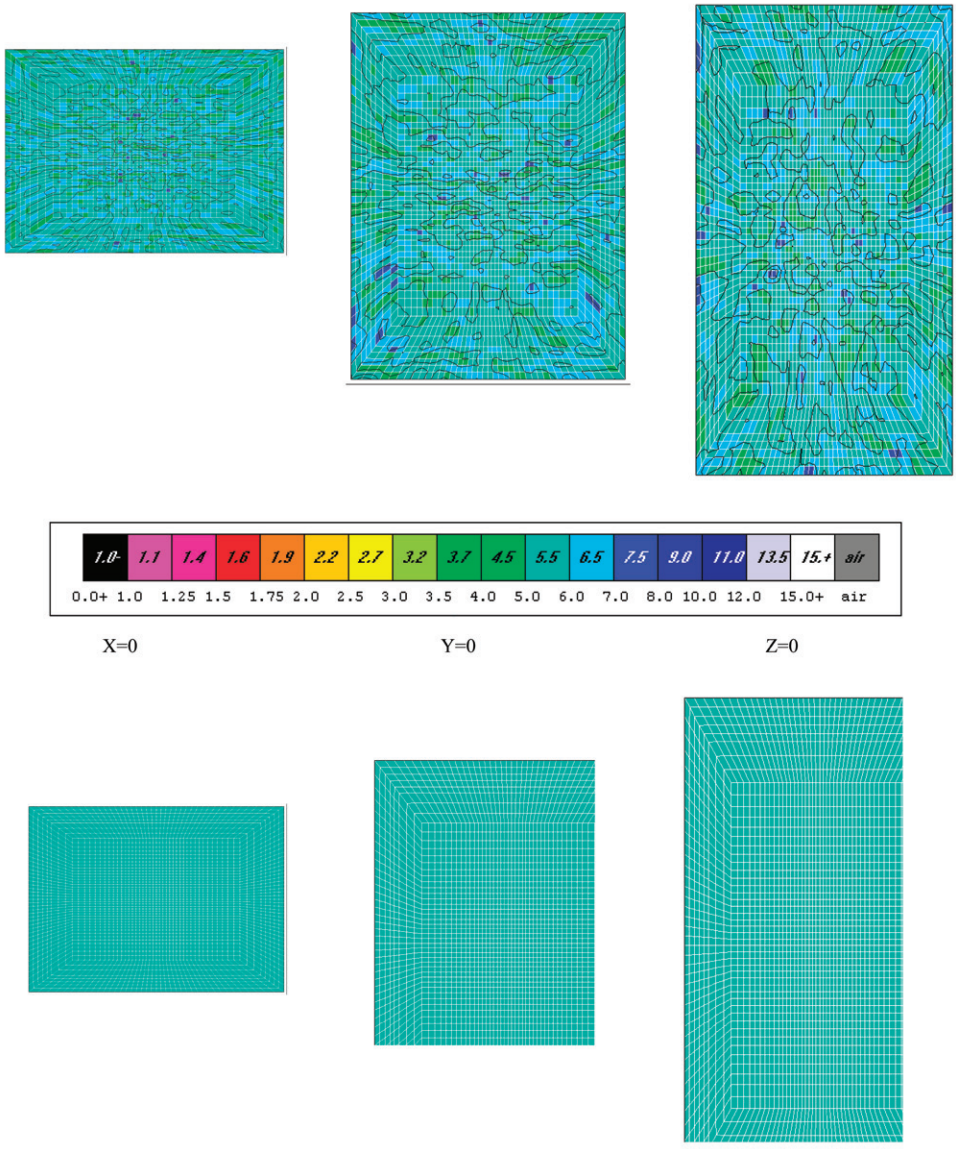

Figure 13 — Preexcavation safety factor distributions: (top) random and (bottom) uniform properties.

beyond which values are independent, is quite short in this data set, perhaps less than 0.3 m (1 ft). Because the smallest element dimension is greater than the estimated correlation length, element properties are uncorrelated and the random (Gaussian) assignment of tensile strength produces a reasonable representation of variability in situ.

Reseeding the random number generator will lead to a different assignment of element properties, although the statistical features, including the mean and standard deviation, remain the same as in the original distribution. Each distribution or "realization" would be associated with a different FE result. Although each distribution of element properties would have the same statistical features, some would be much more likely to form a failure path through low-strength elements than others. Estimation of a probability of failure distribution would require thousands of analyses. What an acceptable design probability of failure would be is an open question and one certainly conditioned by a number of factors such as service life, personnel traffic and, more generally, what the consequences of a failure might be. Only a single analysis is done here for the purposes of illustration.

Randomness also poses an interesting question of how to initialize the preexcavation stress field. In a homogeneous rock mass, an estimate of gravity-induced initial vertical stress is specific weight times depth; horizontal stresses are equal and equal to some fraction of the vertical stress. This stress field could simply be assigned according to element center depth or computed with an assignment of self-weight to elements, thus switching gravity on. However, analytical assignment is not valid when the rock mass of interest is nonhomogeneous. In a heterogeneous rock mass, a uniform stress field violates compatibility; a uniform strain field violates equilibrium. Thus, a gravity turn-on is required. A complication occurs in the gravity turn-on procedure and that is in the specification of exterior boundaries. A proper top boundary condition leaves surface nodes free, provided the mesh extends to the surface. A bottom boundary condition would prevent vertical movement of nodes, while allowing lateral motion. The side boundary conditions are problematic, because the usual practice of fixing side nodes in the horizontal direction now influences the resulting stress state, unlike the homogeneous case. If the mesh does not extend to the surface, then the top boundary condition is also problematic.

A method that generates a proper preexcavation stress field in a gravity-loaded heterogeneous rock mass is to apply boundary forces that are statically equivalent to the same forces present in a homogeneous rock mass. Application of these forces ensures equilibrium and compatibility of the preexcavation stress field. A simple test of the method is to apply the subject forces to an unstressed homogeneous rock mass. The resulting stress distribution should be the same as a stress field achieved by analytical assignment.

The preexcavation stress field in this procedure does not need to be caused by gravity alone. Indeed, simple formulas, such as the regression equations in Fig. 4, may be used to generate the required boundary forces. In this case, the preexcavation stress field in the heterogeneous rock mass will be consistent with the given formulas that were derived from actual stress measurements. Interestingly enough, there is variability in stress measurements because of variability in rock properties.

Figure 13 shows element safety factor distributions in homogeneous and heterogeneous rock masses before excavation. The three views are the coordinate planes that pass through the center of the cavern. Uniform properties were assigned in

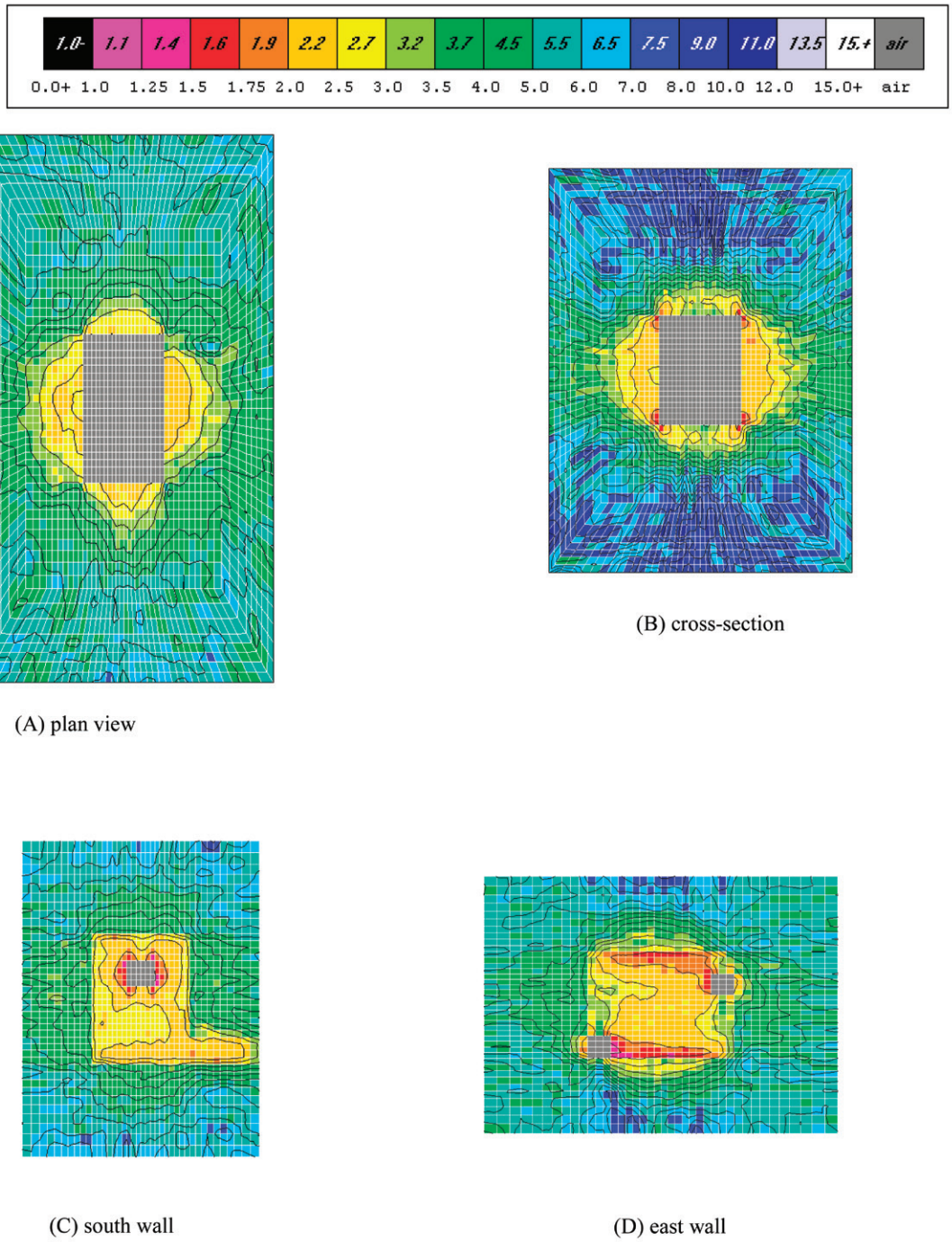

Figure 14 — Post-excavation distributions of element safety factors after random assignment of element properties.

the homogeneous case; random assignment was used in the heterogeneous case. The in situ stress field was generated in accordance with the formulas given previously. The almost uniform element safety factor distribution that ranges from 5.52 to 5.62 is a consequence of the small vertical extent of the mesh relative to depth. In the heterogeneous case, the preexcavation element safety factors range from a low of 3.36 to a high of 8.94. The contours reflect the topography of the distributions. No element failures occurred in either case.

Figure 14 shows element safety factor distribution after excavation in the heterogeneous case. There are no element failures in the heterogeneous case and none in the homogeneous case, and only nine in the scaled, homogeneous case using scale factors of 0.25 and 0.5 for moduli and strengths. In the latter homogeneous case, element failures occur in the skin of entries penetrating the cavern, as one expects. In the heterogeneous case, no element has a safety factor less than 1.3 and none are greater than 14. In the homogeneous case, the range is 1.3 to 12. In both cases, the lowest element safety factors occur in the east wall where the top and bottom drifts enter the cavern. The main difference between the two cases is in the "noisy" pattern that occurs in the heterogeneous case.

In both cases, stress concentration still occurs at the walls of the excavation and is more concentrated where access drifts penetrate the cavern. Thus, while variability makes a difference, in this case, the difference is tolerable.

Role of joints

Joints often play a vital role in the safety and stability of excavations in rock. Indeed, joints make rock mechanics a distinct discipline within the broad domain of solid mechanics. Taking joints into rational and, therefore, reliable account is a central challenge to the rock mechanics community. A simple method in principle is to represent joints in FE analyses by thin elements that are otherwise no different than adjacent rock elements other than in material properties. Of course, joints are expected to be much more compliant and weaker than intact rock between joints. In this way, rigor is achieved within well-developed and understood finite element theory. Very limited success is possible in this simple way, mainly because of the very high joint element aspect ratio that leads to severe numerical difficulties. No success has been achieved when intersecting joints from multiple joint sets are involved. However, with sufficient mesh refinement, which allows many joints to be used to represent joint segments, the aspect ratio obstacle may be negated. Thousands of very small elements are required and ultimately an impossibly large number of elements are needed to directly represent even a small excavation in a jointed rock mass.

A viable FE approach to jointed rock mass mechanics, and one that is rigorous, reliable and practical, is one that uses equivalent properties (Pariseau, 1999). In this approach, a mesh is constructed according to the usual guidelines for obtaining accurate results near excavation walls and for computational efficiency. Joint set data are used to embed joints in elements according to element geometry and joint orientation and spacing. A single element may contain hundreds of intersecting joint segments having very different properties. However, the usual element data are not stored; in effect, joint segments are virtual elements. The need to store thousands of small elements to represent joints is negated in this way. Equivalent elastic moduli are computed for each element in turn. If an element fails, or a joint segment within an element fails or if intact rock in a jointed element fails, then an incremental load path is pursued and the equivalent moduli are updated accordingly. Elastic-plastic, viscoplastic and poroelastic-plastic models have been explored. No equivalent strength properties are required, because the use of influence functions allows for joint failures and for failure of intact rock, all within each ordinary element in the mesh.

When joints are so numerous in an element that one joint segment more or less has little effect on the equivalent properties, then the element is large enough to be considered a representative volume element (RVE). The RVE concept underpins much of the sizeable literature on equivalent properties, especially in the literature on composite materials. Interestingly, materials with a periodic structure based on repetitions of a unit cell exhibit an RVE that is just the unit cell. A patterned brick or stone wall has a periodic structure and a unit cell that is readily defined without the need for including many bricks. The same may be true in well-jointed rock masses, where a regular pattern is created by the joints. Indeed, the joint sets may form a unit cell. Figure 15 shows several sample cubes with joints from each sample set and an example of a unit cell formed by four joint sets at the Homestake site.

A plot of normalized equivalent elastic moduli versus cell size relative to maximum joint set spacing is shown in Fig. 16. The sharp decrease in equivalent moduli occurs just as the sample cube size exceeds maximum joint spacing (Table 3). Equivalent moduli are reduced to less than 20% of laboratory

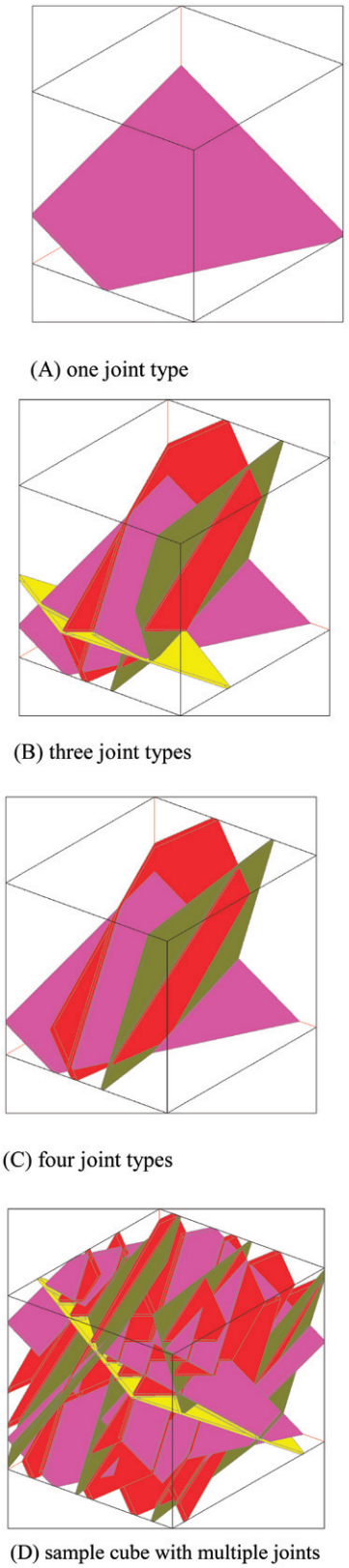

Figure 15 — Sample cube for equivalent properties estimation showing members of the four joint sets. A unit cell is formed by joints from the four sets.

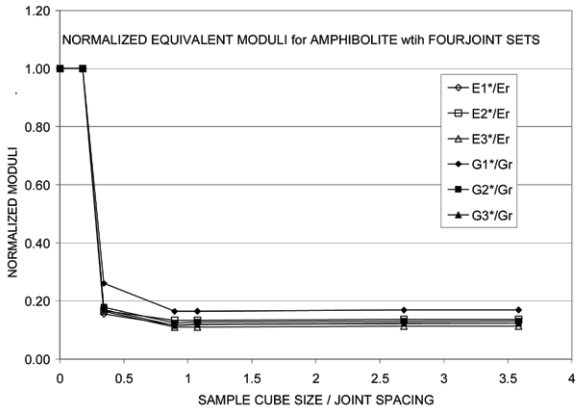

Figure 16 — Equivalent elastic moduli versus sample cube size. Moduli are divided by laboratory values. Distance is divided by maximum joint spacing.

test values, as shown in Fig. 16. In this regard, all elements become fully anisotropic with joint embedment. Generally, the coupling constants that link normal stress and shear strain and shear strain and normal stress are small relative to the Young's and shear moduli. Poisson's ratios range over a set of values, as do the moduli. The process does not impose symmetry; rather, symmetry is used as a check on computations. A 20% reduction in moduli is, coincidentally, roughly the same as the 0.25 scale factor estimated previously from back analyses. If the intact rock moduli were assigned at random, then the equivalent moduli would vary accordingly. In RVE-size elements, this variability may be somewhat masked by the role of joints. In sub-RVE size elements, the variability would be more evident. In these analyses, the RVE size is characterized by a linear dimension of about 2 m (6 ft). Consequently, most of the elements in the mesh are sub-RVE size, while the larger elements near the outer mesh boundaries are RVE size.

Joints create a heterogeneous rock mass; thus, the preexcavation state of stress must be initialized in the same way as the heterogeneous rock mass model associated with random rock properties assignment. Over 970,000 joint segments are embedded in the mesh in this analysis. No element failures occur under application of the preexcavation boundary forces derived from in situ stress measurements, but almost all joint segments fail. After excavation, 31 elements fail, while joint segments continue to fail. Figure 17A shows the preexcavation distribution of element safety factors in the presence of joints in a plan view of the $z = 0$ coordinate plane. Post-excavation views are also shown in Fig. 17. Black elements are failed elements in the figure.

A combination of random assignment of intact rock properties and joint embedment creates a third type of heterogeneous rock mass. While various effects are conveniently separated computationally, in nature, randomness and joints are present simultaneously. However, this possibility was not pursued. Figure 18 presents a brief visual comparison of the effects of scaling, random assignment and joints on the distribution of element safety factors in the east wall of the cavern.

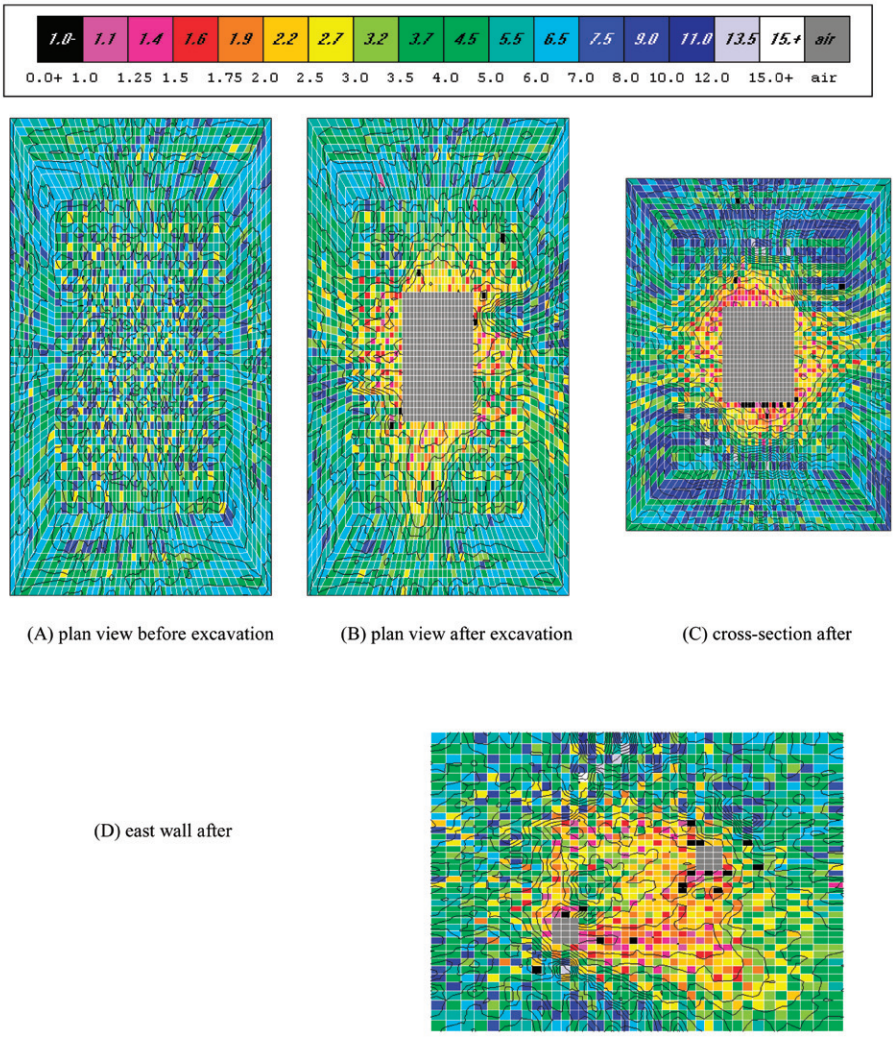

Figure 17 — Element safety factor distributions with joints. (A) $z = 0$ coordinate plane before excavation, (B) $z = 0$ coordinate plane after excavation, (C) $y = 0$ vertical cross-section after excavation and (D) east wall after excavation.

Role of rhyolite and breccia

Rhyolite dikes are present as discontinuous lenses and pods in the west side of the Davis Cavern and, quite recently, a brecciated zone was identified and mapped in the eastern portion of the cavern. The pods and lenses of rhyolite vary in thickness and attitude at the Homestake site. In the Davis Cavern, a thickness of 6.1 m (20 ft), a dip of 50° and a dip direction of 110° were assumed. The breccia zone was assumed to be 2.4 m (8 ft) thick, dipping 80°, with a dip direction of 90°. Rhyolite properties are given in Table 1. Breccia zone properties are unknown, so were assumed to be the same as the rhyolite properties. The reason for this assignment is the evident high strength of the breccia zone that shows no adverse effects on

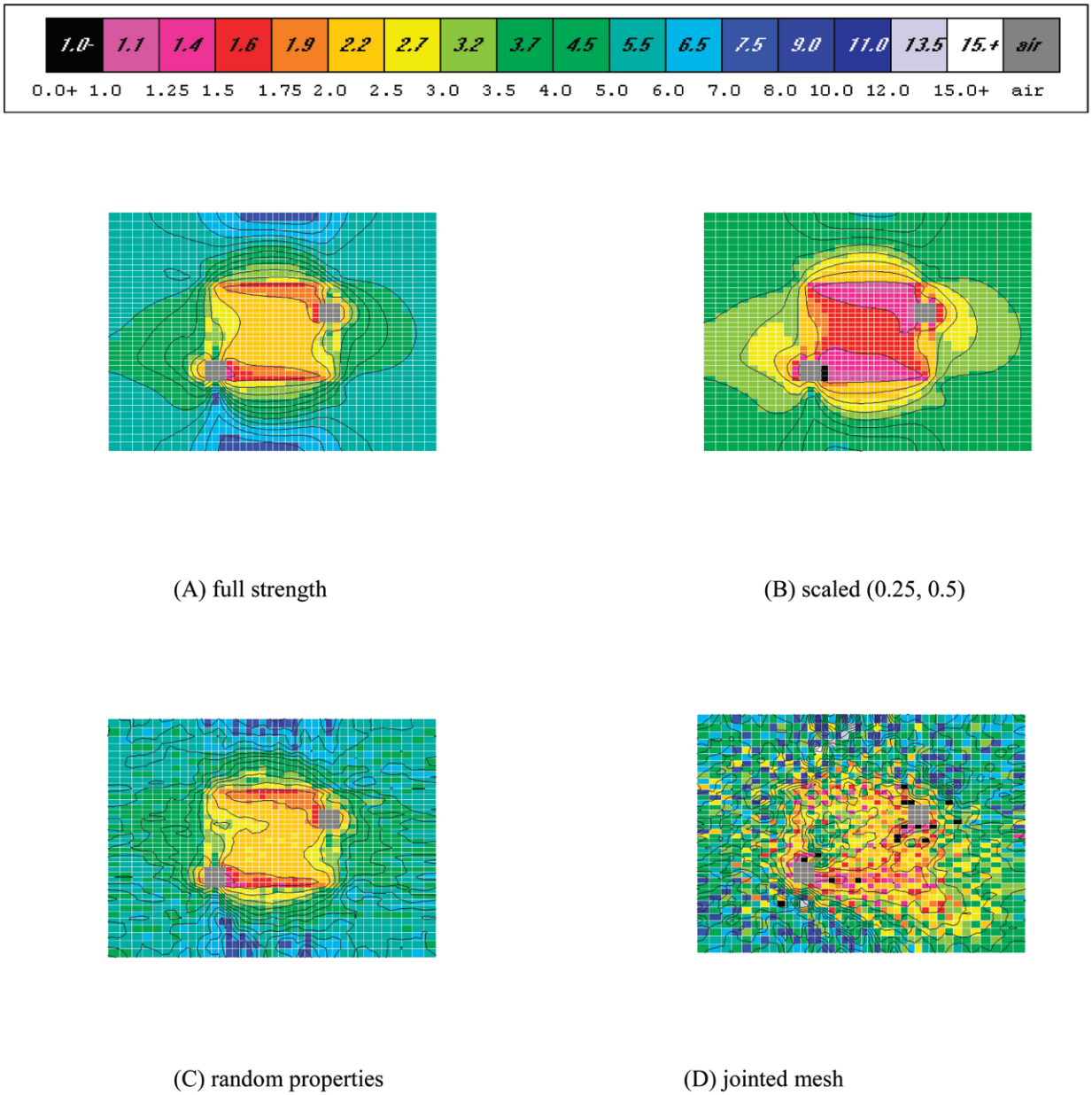

Figure 18 — Comparison of effects of scaling moduli and strengths, random assignment of rock properties and the effects of joints from four sets based on element safety factor distributions after excavation. View is of the east wall, where two access drifts penetrate the cavern.

cavern safety. Base case analyses were done first using uniform properties for amphibolite, rhyolite and breccia. There were 23,714 rhyolite elements (17%) and 14,216 (10%) breccia elements in the mesh. Amphibolite elements were 73%. These percentages are roughly volume percentages. Rhyolite was observed to vary from 8% to 40%, depending on location. Joints were then embedded and the analyses repeated. Random properties were not pursued at this stage of study. In this regard, joints introduce variability of element properties and generate rather "noisy" results, somewhat similar to random assignment of intact properties. Because rhyolite has a lower Young's modulus and Poisson's ratio than amphibolite, but has about the same unconfined compressive and tensile strengths, the rhyolite effect on cavern safety is expected to be small.

Figure 19 shows element safety factor distributions with rhyolite and breccia present (A, B, C) and with joints present as well (a, b, c). Properties of intact rock and joints are uniform, not random, as evident in A, B and C of Fig. 19. Also evident are the rhyolite (wide) and breccia (narrow) zones. Joints are present in a, b and c of Fig. 19, in addition to the rhyolite and breccia zones. Results in Fig. 19, B and C, with rhyolite and breccia may be compared with Fig. 9, B and C, without rhyolite and breccia. Both sets of results are scaled using the same modulus and strength scale factors of 0.25 and 0.50, respectively. The more compliant rhyolite and breccia show elevated safety factor values, as expected in consideration of comparable strengths. Contacts between rhyolite and breccia with amphibolite are entangled and show negligible alteration

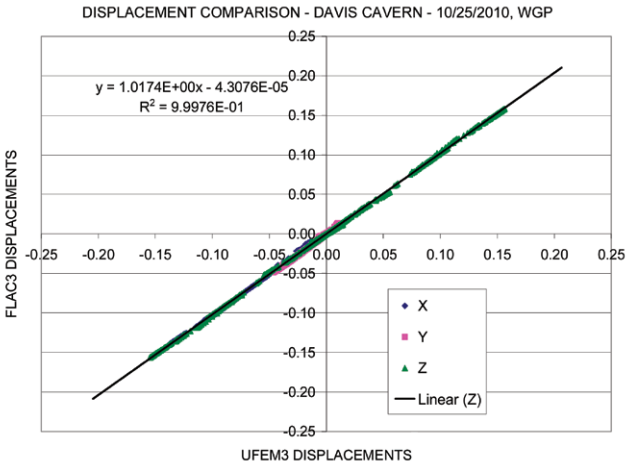

Figure 20 — Displacement component comparison between FLAC3D and UTAH3.

requires failure of intact rock between joints. Evidently, the redistribution of stress induced by excavation in the presence of joints is sufficient to induce some failure between joints. (Failed elements appear black in the figures).

Summary of excavation analyses. The Davis Cavern was excavated in the 1960s and enlarged in 2010 and has stood well through the years. Rising water, cavern flooding and subsequent water drawdown had no apparent effect on cavern stability. Finite element analyses of increasing complexity, including measured variability in elastic moduli and strengths, joints and subsequently rhyolite and breccia zones also show stability. Reducing elastic moduli and strengths from laboratory values using scale factors (multipliers) indicates that factors of 0.25 and 0.50, respectively, are appropriate and in agreement with past rock mechanics investigations. However, incorporation of joints in conjunction with intact rock properties obviates the need for scaling. Mapping measured variability in laboratory rock properties into the finite element rock mass model provides for greater realism.

Blasting effects

Blast damage can reduce the elastic properties of the rockmass around the perimeter of a mine opening and cause a redistribution of peak stresses further into the rockmass. The effect of perimeter damage is addressed here by reducing the elastic modulus in the floor, roof and ribs of a finite difference model of the new Davis Cavern. The rockmass moduli are multiplied by 0.75, 0.5 and 0.25 to simulate varying degrees of damage. Each of these modulus values is then assigned to a model zone around the opening perimeter to simulate damage depths of 0.37, 0.76, 1.43 and 3.90 m (1.2 ft, 2.5 ft, 4.7 ft and 12.8 ft). The effect of rhyolite intrusion with elastic moduli lower than the host rockmass is combined with perimeter damage and also modeled using FLAC3D (Itasca, 2006).

A series of comparisons between FLAC3 and UTAH3 at the outset of the study showed excellent agreement between the two programs for an elastic rockmass. A sample of results is shown in Fig. 20, where a displacement component comparison of 2,000 nodes is made. A comparison of 44,000 nodes in an 84,000-plus node model gave the same results. Although the two codes operate in a very different numerical manner (finite difference versus finite element method), the nearly identical

Table 4 — Distance into the rib and thickness of rhyolite intrusions.

Distance into rib, m (ft)	Width, m (ft)
3.9 (12.8)	1.3 (4.4)
3.9 (12.8)	9.2 (30.2)
7.9 (26.0)	10.1 (33.0)

results indicate reliability of the analyses. Zone (cell) and element stresses also compared quite well, as one might expect from the excellent agreement in displacements. The largest positive and negative displacements are the vertical (z) components.

Numerical model. The enlarged cavern model was 9.1 m (30 ft) wide by 16.8 m (55 ft) long by 12.2 m (40 ft) high. Symmetry was used in the model so that half the width and length of the actual cavern were modeled. The distance from the longitudinal ribs to the boundary perpendicular to these ribs was five times the width of the cavern. Distances from the ribs at the end of the cavern, the mine floor and the mine roof to the respective boundaries were proportioned in the same manner. Displacements at the outside boundaries were fixed in the direction perpendicular to the boundary plane. The mesh contained 80,384 zones and 84,784 nodes. Dimensions of the sides of the zones in the vicinity of the cavern were about 1 ft and became progressively larger to 4.6 m to 9.1 m (15 ft to 30 ft) at the boundaries. Input data were similar, although not identical in every respect to the data used in the FE analyses. Stresses at the midpoint between the mine floor and rib were S_v = 42 MPa (6,093 psi), S_H = 32.14 MPa (4,661 psi), and S_h = 19.32 MPa (2,802 psi) (v = vertical, H = east, h = north, compression positive). The cavern was excavated in one step, as in the FE analyses after path dependency was determined to be negligible.

Laboratory values of intact rock moduli were reduced by a scale factor to obtain rock mass moduli in situ. Strength was not reduced in this initial study, to illustrate that damaged rock measurably affects stress distribution, although the effect of strength reduction is likely to be significant. The scale factor was 0.36 and based on previous back analyses at the Homestake Mine (Pariseau et al., 1995). To simulate various degrees of perimeter damage, amphibolite rock mass moduli were then multiplied by factors of 0.75, 0.5 and 0.25 for distances of 0.37 m, 0.76 m, 1.43 m and 3.9 m (1.2 ft, 2.5 ft, 4.7 ft and 12.8 ft) into the cavern ribs, floor and back.

A rhyolite intrusion was included in the model for each of three amphibolite modulus values representing perimeter damage and four damage distances. Selected results follow. Nodal point coordinates in the model were chosen to create thicknesses that approximated the reported minimum and average measured thicknesses. The locations and thicknesses of the rhyolite are listed in Table 4.

Blasting effects results

Results of the blast damage study are divided into two categories: damage with no rhyolite intrusion present and damage with rhyolite present. The distance of the amphibolite/rhyolite contact from the rib and the thickness of the rhyolite influence the results that are presented here in the form of rib stress as a function of distance into the rib. Compressive stress is negative in this section.

Perimeter damage with no rhyolite intrusion. Plots of

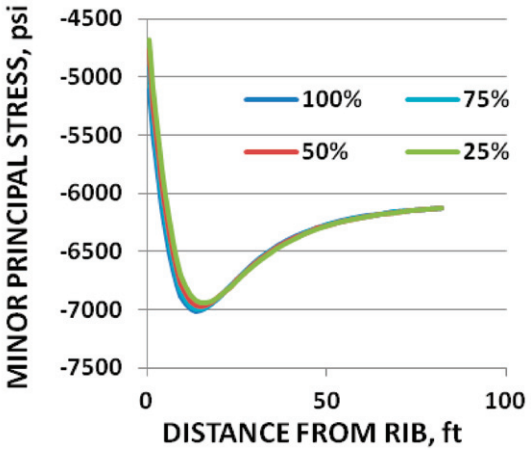

Figure 21 — Distance from rib versus minor principal stress, 0.37 m (1.2 ft) perimeter damage. Rockmass modulus in damaged zone is multiplied by percent in key.

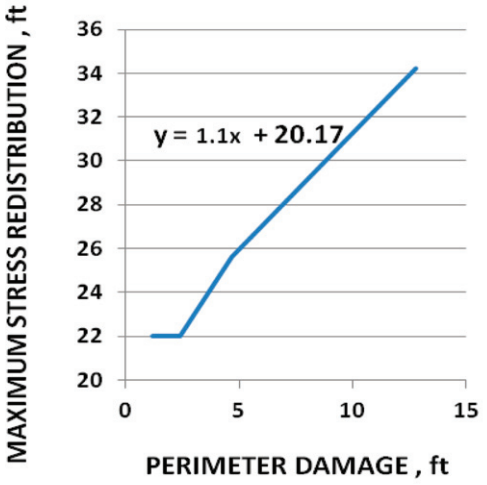

Figure 23 — Maximum stress redistribution distance versus perimeter damage into the cavern rib.

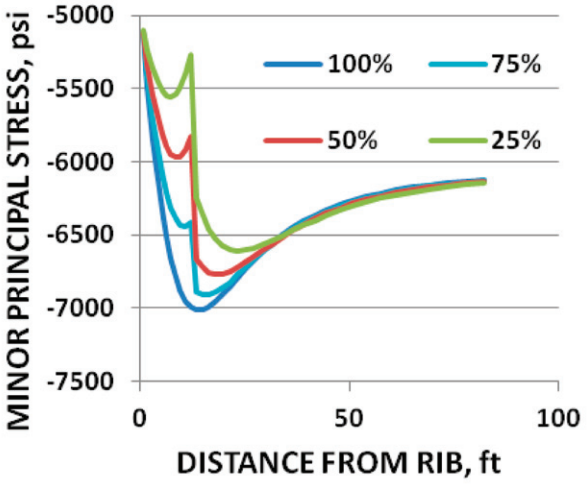

Figure 22 — Distance from rib versus minor principal stress, 3.9 m (12.8 ft) perimeter damage. Rockmass modulus in damaged zone is multiplied by percent in key.

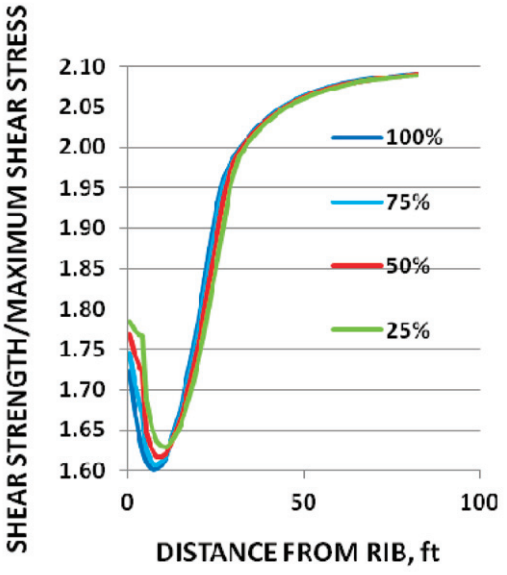

Figure 24 — Distance from rib versus shear strength/maximum shear, 1.43 m (4.7 ft) perimeter damage. Rockmass modulus in damaged zone is multiplied by percent in key.

the distance into the rib along a horizontal line from the center of the cavern, at the midpoint between the floor and back, versus minor principal stress (largest compressive stress or "peak" stress) for minimum and maximum perimeter damage distances of 0.37 m and 3.9 m (1.2 ft and 12.8 ft) are shown in Figs. 21 and 22. Blast damage, simulated by reducing the elastic moduli, results in a redistribution of stress from the rock near the face to undamaged rock further away from the face. As damage severity increases, the minor principal stress at any given distance into the rib decreases in absolute value. This trend reverses at a given distance d, depending on the depth of the damage zone. The parameter d is independent of the severity of damage and increases linearly as a function of damage distance into the rib greater than or equal to 0.76 m (2.5 ft), as shown in Fig. 23.

The distance of maximum stress redistribution into the rib is significant compared to the depth of perimeter damage. This is illustrated in Fig. 24, which is a plot of shear strength/maximum shear stress plotted against distance into the rib.

Effect of rhyolite intrusion on stress distribution. The introduction of a rhyolite intrusion located from 3.9 m to 13.1 m (12.8 ft to 43 ft) into the rib causes a stress concentration in the amphibolite at the amphibolite/rhyolite interface located at 3.7 m (12.1 ft). The stress at this point for the case of 75% of the rock mass modulus assigned to the damaged zone is -50.9 MPa (-7,378 psi) and -47.75 MPa (-6,926 psi) without intrusion, as shown in Figs. 25 and 26. Blast damage in the amphibolite rib causes a stress transfer from the damage zone to the undamaged amphibolite. The transfer distance increases with an increase in both the size of the damage zone and damage severity; however, the maximum stress in the amphibolite decreases with an increase in the size of the damage zone and damage severity.

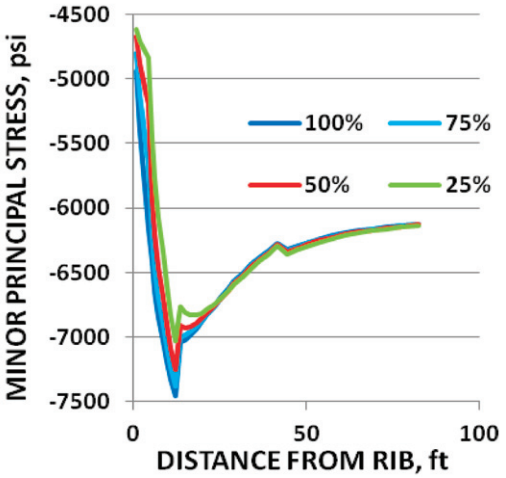

Figure 25 — Distance from rib versus minor principal stress, 1.43 m (4.7 ft) perimeter damage, rhyolite intrusion from 3.9 m to 13.1 m (12.8 ft to 43 ft) from rib. Rockmass modulus in damaged zone is multiplied by percent in key.

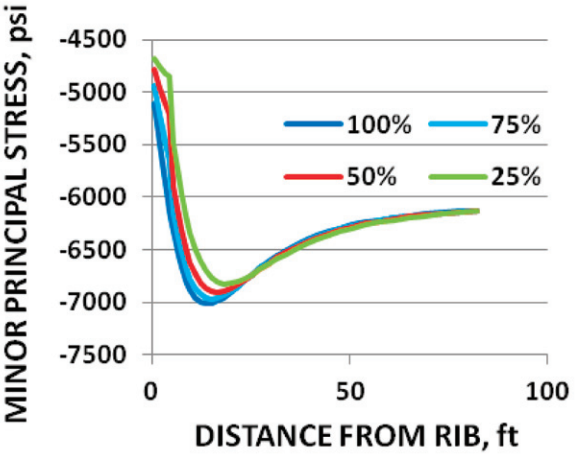

Figure 27 — Distance from rib versus minor principal stress, 1.43 m (4.7 ft) perimeter damage, rhyolite intrusion from 3.9 m to 5.24 m (12.8 ft to 17.2 ft) from rib. Rockmass modulus in damaged zone is multiplied by percent in key.

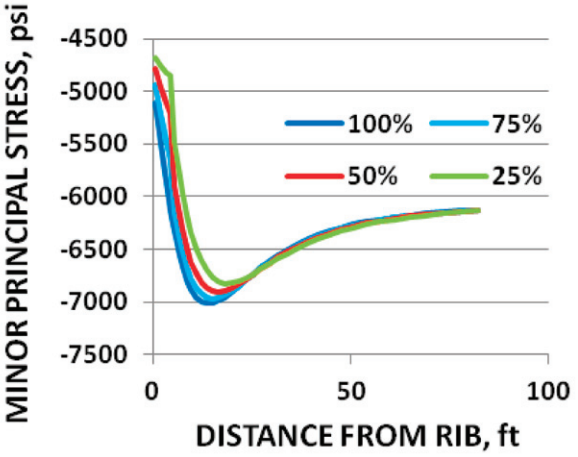

Figure 26 — Distance from rib versus minor principal stress, 1.43 m (4.7 ft) perimeter damage. Rockmass modulus in damaged zone is multiplied by percent in key.

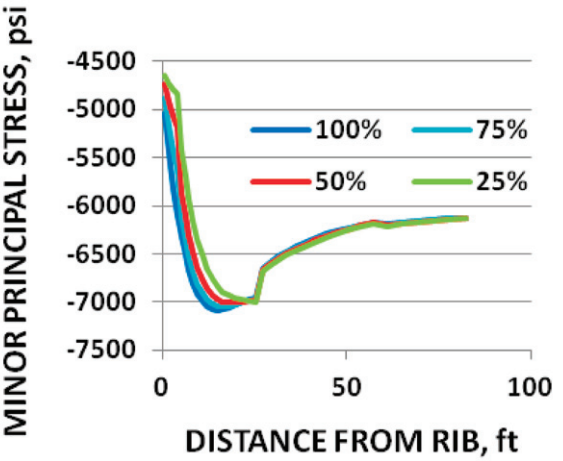

Figure 28 — Distance from rib versus minor principal stress, 1.43 m (4.7 ft) perimeter damage, rhyolite intrusion from 7.9 m to 18 m (26 ft to 59 ft) from rib. Rockmass modulus in damaged zone is multiplied by percent in key.

Decreasing the width of the rhyolite intrusion from 9.2 m to 1.34 m (30.2 ft to 4.4 ft) decreases the maximum stress in the stiffer, undamaged amphibolite rib. For the case of 75% of the rockmass modulus assigned to the damage zone, peak stress concentration is reduced from -50.87 MPa (-7,378 psi) to -49.36 MPa (-7,159 psi) or 3%, as shown in Fig. 27.

Shifting a 9.1-m-wide (30-ft-wide) rhyolite intrusion from 3.9 m to 7.9 m (12.8 ft to 26 ft) into the rib of the amphibolite rockmass decreases the maximum stress as shown in Fig. 28. For the case when 1.43 m (4.7 ft) of rib damage is modeled with 75% of the rockmass modulus and the intrusion is located 3.9 m to 13.1 m (12.8 ft to 43 ft) into the rib, the maximum stress is -50.87 MPa (-7,378 psi). The maximum stress is -38.61 MPa (-7,050 psi) when the intrusion is located from 7.9 m to 18 m (26 ft to 59 ft) from the rib. The decrease in stress is 4%.

Zone failure in the damaged perimeter causes additional stress reduction, as shown in Fig. 29. Redistributed stresses occur in both the damaged perimeter and intact rock further into the rib. The laboratory modulus was used for undamaged amphibolite. Cohesion and angle of internal friction equal to 20.82 MPa (3,020 psi) and 58.1 degrees, respectively, were used for the Mohr/Coulomb strength parameters.

Summary of blasting effects. Blast damage, simulated by reducing the elastic moduli of the rockmass, results in a redistribution of stress from the rock near the face to undamaged rock further away from the face. As damage severity increases, the minor principal stress at a given distance into the rib decreases in absolute value. This trend reverses at a given distance d, depending on the depth of the damage zone. The parameter d is independent of the severity of damage and increases linearly as a function of damage distance into the rib for damage distances equal to or greater than 0.76 m (2.5 ft).

Decreasing the width of the rhyolite intrusion decreases the

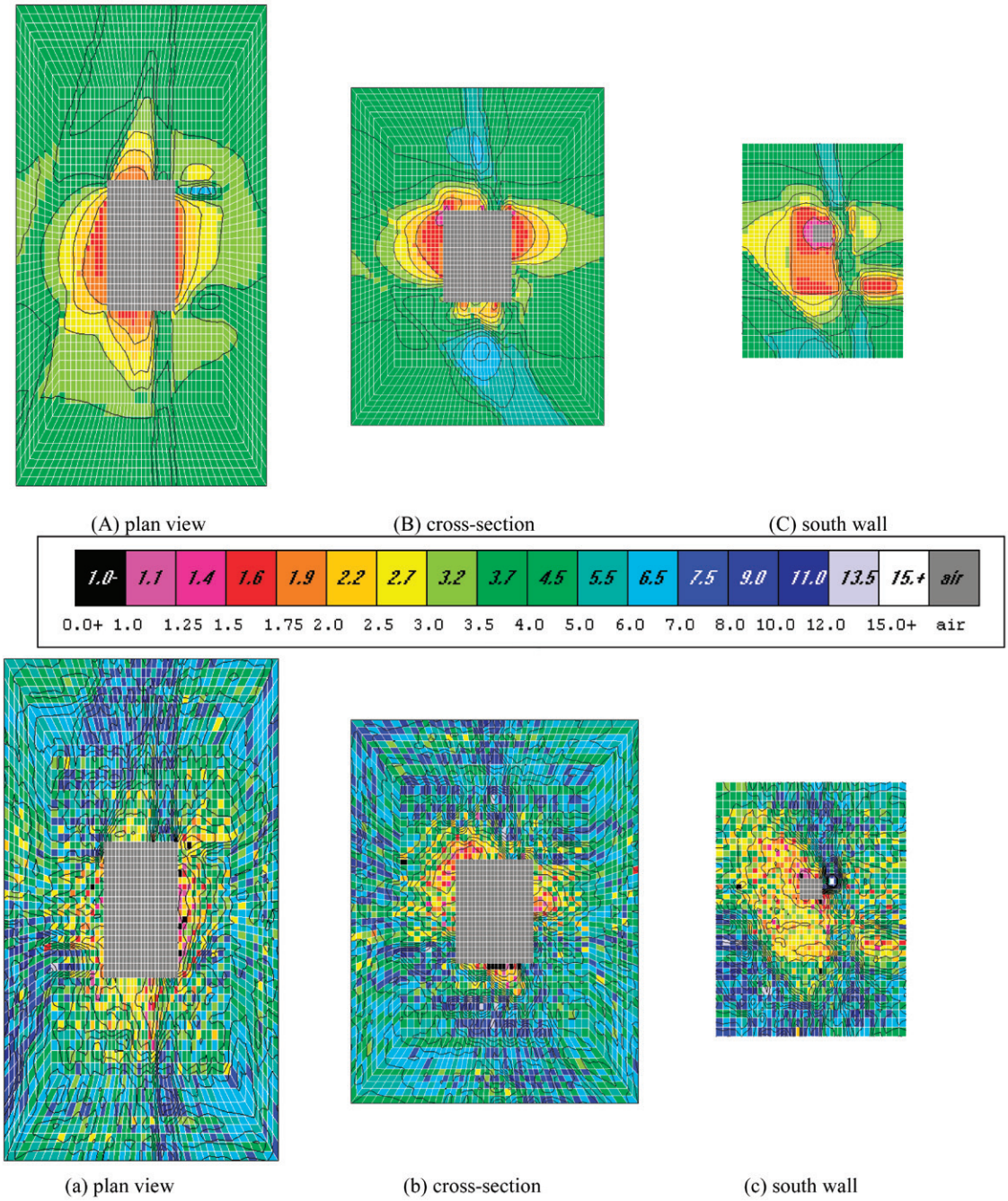

Figure 19 — Element safety factor distributions with easterly dipping rhyolite and breccia zones present using scale factors A, B, C: 0.25 and 0.50; a, b, c not scaled but with joints.

and, thus, are quite strong.

Results in Fig. 19, a and b, with joints and rhyolite and breccia may be compared with the element safety factor distributions in Fig. 17, B and C, without rhyolite and breccia but with joints. The "noisy" pattern caused by joints is evident in both sets of results. The effect of rhyolite and breccia zones is also evident. Again, the element safety factors are elevated relative to the case of amphibolite only, although the variability introduced by joints tends to mask the trend.

In both cases with joints, there are 957,043 joint segments in the mesh. Generation of an initial state of stress that is at equilibrium and a companion state of strain that is compatible and linked to the stresses is done at the outset. This process is essential to achieve a proper initial state of stress and to avoid undetected effects on subsequent analyses. These effects would be additional stress, strain and displacement changes necessary to equilibrate the out of equilibrium and lack of compatibility in the preexcavation (initial) state. The same requirement is true whenever different rock types are present, even in the absence of joints. During the initialization process here, almost every joint segment in the mesh is deformed beyond the elastic limit and yields. In retrospect, this result should not be surprising, because joints appear as a consequence of intact rock fracture. Joints continue to yield during subsequent excavation analyses. No macroelement yielded during generation of the initial stress state. However, in the case of amphibolite, only 9,060 elements failed. When rhyolite and breccia were included in the model, about 8,651 elements failed. Element failure in this context

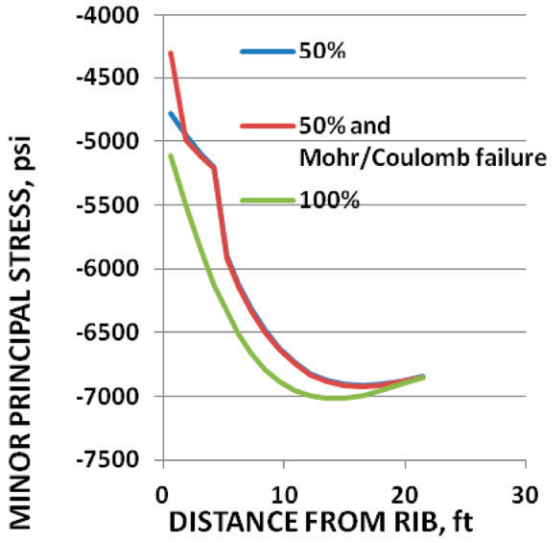

Figure 29 — Distance from rib versus minor principal stress, 1.43 m (4.7 ft) perimeter damage and 0.3 m (1 ft) rib failure. Rockmass modulus in damaged zone is multiplied by percent in key.

magnitude of the stress concentration in the amphibolite rockmass. In the case of 75% of the rockmass modulus assigned to the damage zone, peak stress concentration is reduced by 4%.

Shifting a 9-m- (30-ft)-wide rhyolite intrusion further into the rib of the amphibolite rockmass decreases the magnitude of the maximum stress.

Zone failure in the cavern's damaged perimeter causes stress reduction, in addition to the stress reduction attributed to perimeter damage alone. Redistributed stresses occur in both the damaged perimeter zone and the undamaged rock further into the rib.

Conclusion

The Davis Detector cavern was excavated in Precambrian amphibolite off the 4850 Level (feet below surface) of the former Homestake Mine for the study of solar neutrinos. The 9.1 x 16.8 x 9.7-m-high cavern has stood well for more than 45 years and was recently enlarged. Rhyolite dikes, strong breccia zones and joint sets were incorporated into finite element analyses using UTAH3 for evaluating cavern safety and stability. Measured variability in laboratory rock properties was also incorporated into the analyses as a step towards greater realism. The main objective was to estimate lower bounds to properties of the jointed rock mass about the cavern. Blast wall damage was included in the study using the finite difference code FLAC3D. Comparison of results in the elastic domain showed excellent agreement between computer codes (UTAH3 and FLAC3D).

The main conclusions are: (1) if rock mass moduli and strengths used in analysis are obtained using scale factors, then scale factors for moduli and strengths of 0.25 and 0.50 are reasonable, (2) if joints are included in analysis, then measured stiffnesses and strengths of joints and intact rock between joints may be used, and scaling is unnecessary, (3) inclusion of observed variability in rock properties is important, (4) inclusion of major geologic features such as rhyolite dikes and breccia zones is a step towards reality and more useful design guidance, (5) blast damage affects cavern wall stress in a site-specific, quantifiable way and should be minimized. These results should provide useful design guidance for much larger water Cherenkov detector caverns (perhaps 65 m in diameter and 85 m high) being considered for excavation off the same 4850 Level. Although these results are site-specific, the procedures and computer codes have sufficient generality to be useful across a wide spectrum of site conditions found elsewhere.

Acknowledgments

This research was supported in part by the National Science Foundation under grants PHY-0717003 and PHY-0940801. Support of personnel of the Sanford Underground Science and Engineering Laboratory and the many members of the DUSEL team is gratefully acknowledged, especially Dr. Z. Hladysz, who has returned to teaching and research at the South Dakota School of Mines and Technology. The views and conclusions expressed in this paper are those of the authors and are not necessarily the official views or policies of NIOSH, Office of Mine Safety and Research, the Sanford Underground Science and Engineering Laboratory at Homestake, or the University of Utah.

References

Golder Associates, 2010a, Preliminary Design Interim Report #3. Engineering and Design Services for Excavation - DUSEL.

Golder Associates, 2010b, Geotechnical engineering services in-situ stress measurement – Deep Underground Science and Engineering Laboratory.

Griffiths, D.V. and G. A. Fenton, Eds., 2007, *Probabilistic Methods in Geotechnical Engineering*, SpringerWien, NY.

Hladysz, Z.J, Callahan, G.D., Popielak, R., Weinig, W., Randolph-Lear, C., Pariseau, W.G., and Roggenthen, W., 2011, "Site investigations and geotechnical assessment for the construction of the Deep Underground Science and Engineering Laboratory at the former Homestake Mine," Society for Mining, Metallurgy and Exploration 2011 SME Preprints CD (11-046), Denver, CO.

Itasca Consulting Group, Inc., 2006, FLAC3D – Fast Lagrangian Analysis of Continua in 3 Dimensions.

Mitchell, S.T., 2009, "Nuggets to neutrinos: the Homestake story," XLibris, www.XLibris.com, p. 553.

Pariseau, W.G., 1967, "The post-yield mechanics of rock and soil," *Mineral Industries Bulletin*, The Pennsylvania State University, Vol. 36.

Pariseau, W.G., 1972, "Plasticity theory for anisotropic rocks and soils," *Proceedings of the 10th U.S. Symposium on Rock Mechanics*, K.E. Gray, ed., AIME/SME, NY, pp. 267-295.

Pariseau, W.G., 1985, "Research study on pillar design for vertical crater retreat (VCR) mining," Bureau of Mines Contract Report J0215043.

Pariseau, W.G., Johnson, J.C., McDonald, M.M., and Poad, M.E., 1995, *Rock Mechanics Study of Shaft Stability and Pillar Mining, Homestake Mine, Lead, SD*, USBM R9576 Part 2 - Mine Measurements and Confirmation of Premining Results.

Pariseau, W.G., Johnson, J.C., McDonald, M.M., and Poad, M.E., 1996, *Rock Mechanics Study of Shaft Stability and Pillar Mining, Homestake Mine, Lead, SD*, USBM R9618 Part 3 - Geomechanical Monitoring and Modeling Using UTAH3.

Pariseau, W.G., 1999, "An equivalent plasticity theory for jointed rock masses," *Int J. Rock Mech. Mng. Sci.*, Vol. 36, No.72, pp. 907-918.

Pariseau, W.G., Byrnes, R.W., Cefalo, R.J., and Schumacher, F.P., 2010, *Laboratory Measurements of Elastic Moduli and Strengths of Rhyolite and Amphibolite from Homestake/DUSEL, Lead, SD*. Department of Mining Engineering, University of Utah.

Singh, M.M., 1981, "Strength of rock," *Physical Properties of Rocks and Minerals*, Y.S. Touloukian, W.R. Judd, and R.F. Roy, eds., Hemisphere Publishing Corporation, N.Y., pp 83-121.

Slaughter, A.L., 1968, "The Homestake Mine," *Ore Deposits in the United States, 1933-1967*, J.D. Ridge, ed., Vol. 2, AIME, N.Y., pp. 1336-1459.